

# Effect of Fluorine Content in Thienothiophene-Benzodithiophene Copolymers on the Morphology and Performance of Polymer Solar Cells

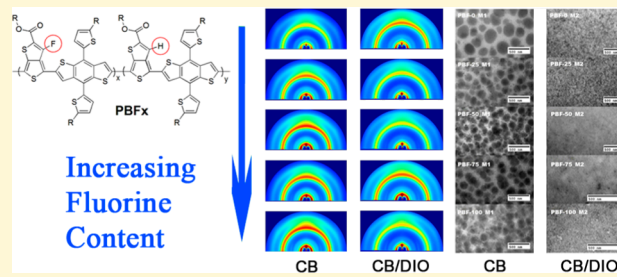
Peng Liu,<sup>†,‡</sup> Kai Zhang,<sup>†,‡</sup> Feng Liu,<sup>†,§</sup> Yaocheng Jin,<sup>‡</sup> Shengjian Liu,<sup>‡</sup> Thomas P. Russell,<sup>\*,§</sup> Hin-Lap Yip,<sup>\*,‡</sup> Fei Huang,<sup>\*,‡</sup> and Yong Cao<sup>‡</sup>

<sup>†</sup>Institute of Polymer Optoelectronic Materials and Devices, State Key Laboratory of Luminescent Materials and Devices, South China University of Technology, Guangzhou 510640, People's Republic of China

<sup>§</sup>Department of Polymer Science and Engineering, University of Massachusetts Amherst, Massachusetts 01003, United States

## Supporting Information

**ABSTRACT:** A new family of polythienothiophene-*co*-benzodithiophene copolymers with different amounts of fluorine decoration ( $\text{PBF}_x$ ) had been successfully synthesized. Detailed structure–property investigations covering physical properties, morphology, and solar cell performance with respect to the fluorine content in the polymers were performed by a series of structural characterization techniques. A PCE of 8.75% was obtained with the highest fluorinated polymer; the morphological trends, as well as the crystalline structure, were also investigated, shedding light on this important material modification.



## INTRODUCTION

Polymer solar cells (PSCs) have attracted much attention due to their potential in flexible, lightweight, and low-cost solar energy harvesting devices.<sup>1,2</sup> One of the key strategies to improve PSCs is to develop better light-harvesting conjugated polymers with desired optical, electronic, and electrical properties. Therefore, different classes of conjugated polymers such as homopolymers,<sup>3</sup> donor–acceptor (D–A) conjugated polymers,<sup>4–9</sup> quinoid polymers,<sup>10,11</sup> two-dimensional polymers<sup>12,13</sup> and other structural polymers have been synthesized and studied for PSC applications. By fine-tuning the chemical structures, the energy levels and bandgaps of the polymers can be effectively tuned to optimize the PSC performance. For example, introduction of electron-withdrawing fluorine atoms on the backbone of the conjugated copolymers can simultaneously increase both the electron affinity (EA) and ionization potential (IP) of the polymer with a deepening of both the lowest unoccupied molecular orbital (LUMO) and the highest occupied molecular orbital (HOMO) without affecting the bandgap of the polymer significantly.<sup>14–28</sup> As a result, the desired light harvesting properties can be retained while the deepened HOMO level leads to increased open-circuit voltage ( $V_{oc}$ ) of the polymer:fullerene bulk-heterojunction(BHJ) cells.<sup>29</sup> Recent studies also suggested that the introduction of fluorine atoms in appropriate locations of the polymer can enhance the internal dipole within the polymer, thus providing extra driving forces to improve the exciton dissociation efficiency in the BHJs, leading to improved short-circuit currents ( $J_{sc}$ ) and fill factors (FF).<sup>30–32</sup> These collective effects

result in polymer solar cells with very high power conversion efficiencies (PCE) of 7–9%.<sup>33–36</sup>

In conjunction with the development of more efficient conjugated polymers through the above-mentioned chemical modification strategies, optimization of the morphology of the BHJ is also required in order to achieve the anticipated improvement in PSC performance.<sup>37</sup> Unfortunately, achieving the desired nanoscale phase separation of the polymer and fullerene in the BHJ film is not trivial and it depends on many parameters, including processing conditions and solvents, substrate wetting properties, compositions of the mixture comprising the active layer, and annealing (thermal and solvent) conditions. Subtle modifications of the chemical structure of the polymers can also markedly alter the surface energies, segmental interactions, and segment rigidity, all of which can influence the morphology of the resultant active layer and the distribution of components within the active layer and at interfaces.<sup>14,17,28,38</sup> As a result, the current approach to exploit the property of new materials for PSC applications is largely proceeded by painstaking device optimization. There is a strong need to systematically study the structure–property–performance relationship of new polymers and establish rational design criteria for developing even better organic photovoltaic materials.

In this study, we describe the synthesis of a series of polythienothiophene-*co*-benzodithiophene based polymers with

Received: March 12, 2014

Revised: April 14, 2014

Published: April 14, 2014



different fluorine content ( $\text{PBF}_x$ ), a systematic study of their optical, electronic, and electrical properties and the characteristics of PSCs based on these polymers. A detailed structural analysis of these polymers in the BHJ films was performed using transmission electron microscopy (TEM), grazing incidence X-ray diffraction (GIXD), and resonant soft X-ray scattering (RSoXS) to elucidate the influence of fluorine content on the morphology of the active layer. From these studies, a structure–property–performance relationship was established, providing materials design criteria for new conjugated polymers for photovoltaic applications.

The polythienothiophene-*co*-benzodithiophene-based polymers were chosen for this study due to their high PSC performance with PCE of 7–9%.<sup>19,35,36,39–41</sup> By replacing the commonly used alkyl- or alkoxy-based side chain with the alkylthiophene one on the benzodithiophene unit, the resulting polymers showed narrower bandgaps and improved charge transport properties owing to the extended conjugation of the polymer. It is interesting to note that this such modification also deepened the HOMO level of the polymer.<sup>35,42,43</sup> Therefore, a new series of polymers ( $\text{PBF}_x$ ) were synthesized based on the copolymerization of the alkylthiophene-substituted benzodithiophene (BDT-T) unit with different feed-ratios of the thienothiophene (TT) and fluorinated thienothiophene (TT-F) unit,<sup>44–46</sup> so as to control the fluorine content in the polymer in a systematic manner (Figure 1). It

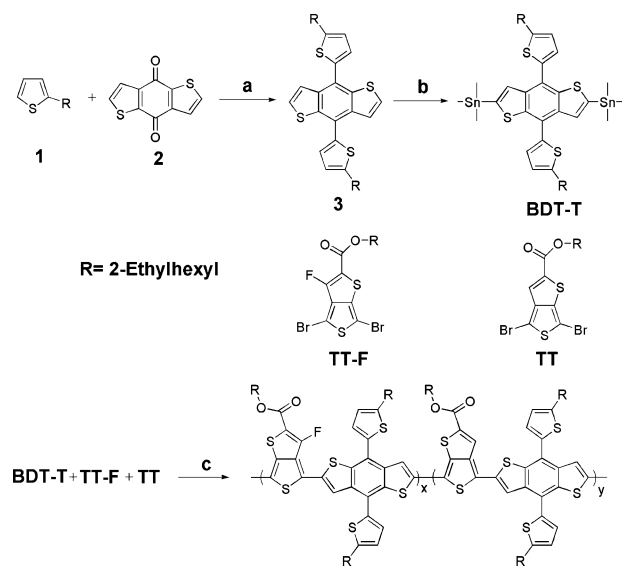


**Figure 1.** Synthesis of  $\text{PBF}_x$  series polymers. (a) *n*-BuLi, THF, 0 °C, then 50 °C, 1 h; then compound 2, 50 °C, 1 h; then  $\text{SnCl}_2/\text{HCl}/\text{H}_2\text{O}$ , ambient temperature, 1.5 h; (b) *n*-BuLi, THF, ambient temperature, 2 h; then  $\text{Me}_3\text{SnCl}$ , ambient temperature, overnight; (c)  $[\text{Pd}(\text{PPh}_3)_4]$ , toluene/DMF (10:1), reflux, 42 h.

was found that the morphologies of the polymer:fullerene BHJ films strongly depend on the fluorine content of the polymers with a reduction in the size scale of phase separation with increasing fluorine content. The best device performance was obtained from the polymer with the highest fluorine content where a PCE of 8.75% was found. The improved performance not only arises from the decreased size scale of the BHJ morphology but also to the enhanced  $V_{\text{oc}}$  and FF arising from the increased HOMO level of the polymer and more balanced charge transport properties in the BHJ film, respectively.

## EXPERIMENTAL SECTION

**Materials.** 2-(2-ethyl-hexyl)thiophene (**1**) and 4,8-dehydrobenzo[1,2-b:4,5-b']dithiophene-4,8-dione (**2**) were synthesized according to a previously reported method.<sup>47,48</sup> 2-ethylhexyl-4,6-dibromothieno[3,4-b]thiophene-2-carboxylate (**TT**) was purchased from 1-Material Inc.; 2-ethylhexyl-4,6-dibromo-3-fluorothieno[3,4-b]thiophene-2-carboxylate (**TT-F**) was purchased from Suna Tech Inc. All of these chemicals were used as received. Tetrahydrofuran (THF) was dried over Na/benzophenoneketyl and freshly distilled prior to use. The other materials were commercially available and used as received.

**4,8-bis(5-(2-ethylhexyl)thiophen-2-yl)benzo[1,2-b:4,5-b']dithiophene (**3**).** Using a 150 mL argon-purged flask, *n*-butyllithium (2.5 M in hexane, 13.2 mL, 33 mmol) was added dropwise to a solution of compound **1** (5.88 g, 30 mmol) in THF (30 mL) at 0 °C. The mixture was then warmed to 50 °C and stirred for 1 h. Subsequently, 4,8-dehydrobenzo[1,2-b:4,5-b']dithiophene-4,8-dione (2.16 g, 10 mmol) was added to the reaction mixture, which was then stirred for 1 h at 50 °C. After cooling the reaction mixture to ambient temperature, a mixture of  $\text{SnCl}_2 \cdot 2\text{H}_2\text{O}$  (18 g, 80 mmol) in 10% HCl (32 mL) was added and the mixture was stirred for additional 1.5 h, after which it was poured into ice water. The mixture was extracted with petroleum ether twice and the combined organic phases were concentrated to obtain the crude compound **3**. Further purification was carried out by column chromatography on silica gel using petroleum ether as the eluent to obtain pure compound **3** as pale yellow viscous liquid (4.1 g, yield 71%). <sup>1</sup>H NMR ( $\text{CDCl}_3$ , 300 MHz), *d*: 7.66 (d, 2 H), 7.46 (d, 2 H), 7.30 (d, 2 H), 6.90 (d, 2 H), 2.88 (d, 4 H), 1.75 (m, 2 H), 1.53–1.18 (br, 16 H), 0.92–0.83 (m, 12 H) ppm. <sup>13</sup>C NMR ( $\text{CDCl}_3$ , 75 MHz), *d*: 145.20, 139.06, 137.49, 136.43, 127.61, 127.31, 125.32, 124.01, 123.29, 41.54, 34.33, 32.53, 29.41, 25.83, 23.04, 15.66, 11.01 ppm. MS (APCI, *m/z*): calcd. for  $\text{C}_{34}\text{H}_{42}\text{S}_4$  [M + 1]<sup>+</sup>, 579.2; found, 579.6.

**2,6-Bis(trimethyltin)-4,8-bis(5-(2-ethylhexyl)thiophen-2-yl)benzo[1,2-b:4,5-b']dithiophene (BDT-T).** A solution of compound **3** (4.23 g, 7.32 mmol) in THF (30 mL) at 0 °C was placed in a 150 mL argon purged flask, and then *n*-butyl lithium (1.6 M in hexane, 16 mL, 25.6 mmol) was added. The reaction mixture was then stirred for 2 h at ambient temperature. Subsequently, chlorotrimethylstannane (1.0 M in hexane, 33 mL, 33 mmol) was added and the mixture was stirred overnight at ambient temperature. Then, the mixture was extracted by dichloromethane and the combined organic phase was concentrated to obtain compound BDT-T. Further purification was carried out by recrystallization using hexane/ethanol to obtain the pure compound BDT-T as a light-yellow solid (3.28 g, yield 49%). <sup>1</sup>H NMR ( $\text{CDCl}_3$ , 300 MHz), *d*: 7.68 (s, 2 H), 7.31 (d, 2 H), 6.90 (d, 2 H), 2.87 (d, 4 H), 1.73 (m, 2 H), 1.53–1.35 (br, 16 H), 0.95 (m, 12 H), 0.39 ppm (s, 18 H). <sup>13</sup>C NMR ( $\text{CDCl}_3$ , 75 MHz), *d*: 145.40, 143.28, 142.25, 138.00, 137.33, 131.19, 127.54, 125.31, 122.41, 41.58, 34.26, 32.52, 28.98, 25.81, 23.05, 15.43, 10.99, 8.33 ppm. MS (APCI, *m/z*): calcd. for  $\text{C}_{40}\text{H}_{58}\text{S}_4\text{Sn}_2$  [M + 1]<sup>+</sup>, 904.4; found, 904.0.

**Synthesis of Polymers.** The comonomer BDT-T (0.25 mmol), TT, TT-F were mixed in 5 mL of toluene and 0.5 mL of DMF. After being purged with argon for 15 min,  $[\text{Pd}(\text{PPh}_3)_4]$  (10 mg) was added as the catalyst, and the mixture was then purged with argon for 5 min. The reaction mixture was stirred and heated to reflux for 42 h. Then, 2-(tributylstannyl)thiophene and 2-bromothiophene were added

to end-cap the polymer chain. The reaction mixture was cooled to room temperature and dropped into methanol. The polymer was precipitated and then collected by filtration. The polymer was subjected to Soxhlet extraction with methanol, acetone, and hexane. The solid was dried under vacuum. After drying in the vacuum drying oven, the polymer was dissolved in toluene, then the Pd-thiol gel (Silicycle Inc.) (30 mg) was added and the solution was stirred for 2 h, followed by silica-gel chromatography with toluene eluent. The polymer was reprecipitated using methanol and dried. Finally, PBF series polymers were obtained as dark purple solid.

The comonomer feed ratios of TT to TT-F are 100:0, 75:25, 50:50, 25:75, and 0:100, and the corresponding copolymers were named PBF0, PBF25, PBF50, PBF75, and PBF100 respectively.

PBF0: Yield (75%). GPC:  $M_n = 34.1$  kDa,  $M_w = 75.1$  kDa, PDI = 2.2.  $T_d = 365$  °C.

PBF25: Yield (72%). GPC:  $M_n = 51.6$  kDa,  $M_w = 123.0$  kDa, PDI = 2.4.  $T_d = 377$  °C.

PBF50: Yield (68%). GPC:  $M_n = 52.6$  kDa,  $M_w = 133.1$  kDa, PDI = 2.5.  $T_d = 373$  °C.

PBF75: Yield (73%). GPC:  $M_n = 40.2$  kDa,  $M_w = 114.8$  kDa, PDI = 2.9.  $T_d = 373$  °C.

PBF100: Yield (80%). GPC:  $M_n = 32.4$  kDa,  $M_w = 86.1$  kDa, PDI = 2.7.  $T_d = 384$  °C.

**Measurements and Characterization.** The  $^{13}\text{C}$  NMR and  $^1\text{H}$  NMR data were collected on a Bruker AVANCE Digital NMR workstation operating at 75 and 300 MHz, respectively. Chemical shifts were reported as  $\delta$  value (ppm) relative to an internal tetramethylsilane(TMS) standard. Gel permeation chromatography (150 °C in 1,2,4-trichlorobenzene) was performed on a Polymer Laboratories PL220 Chromatograph with linear polystyrene as references. Mass spectrometry (MS) data were obtained on a WatersTQD with atmospheric pressure chemical ionization resource (APCI). UV-vis absorption spectra were measured using a HP 8453 spectrophotometer. Thermogravimetric analyzer (TGA) measurements were performed on a Netzsch TG 209 in nitrogen, with a heating rate of 20 °C min<sup>-1</sup>. Differential scanning calorimetry (DSC) measurements were performed on a Netzsch DSC 204. External quantum efficiency (EQE) measurements were taken using a monochromator (Newport, Cornerstone 130) joined to the same xenon lamp and a lock-in amplifier (Stanford Research Systems, SR 830) coupled to a light chopper. The electrochemical cyclic voltammetry experiments were conducted on a CHI800 electrochemical workstation equipped with a graphite electrode coated with thin copolymer film as the working electrode, a saturated calomel electrode (SCE) as the reference electrode, and a Pt sheet counter electrode in a 0.1 M tetrabutylammoniumhexafluorophosphate ( $\text{Bu}_4\text{NPF}_6$ ) acetonitrile solution, at a scan rate of 50 mVs<sup>-1</sup> at room temperature. The potential of the saturated calomel reference electrode was internally calibrated using the ferrocene/ferrocenium redox couple (Fc/Fc<sup>+</sup>), which has a known reduction potential of -4.8 eV. Thus, the IP values of the copolymers were calculated according to the following empirical formulas:<sup>49</sup>

$$\text{IP} = \text{e}[E_{\text{ox}} - E_{\text{ox}}(\text{Fc}/\text{Fc}^+) + 4.80](\text{eV})$$

The  $E_{\text{ox}}$  is the onset oxidation potential vs SCE. It should be pointed out that the reductive curves of the copolymers could hardly be obtained. Therefore, the EA values of the copolymers

were estimated from their optical band gaps and IP values using the equation

$$\text{EA} = \text{IP} - E_g^{\text{opt}}$$

where  $E_g^{\text{opt}}$  denotes the optical band gaps of the copolymers and EA calculated here from the  $E_g^{\text{opt}}$  was approximate values because it ignores the exciton binding energy.<sup>50</sup>

**Characterization of PSCs.** Power conversion efficiencies (PCEs) were measured under a computer-controlled Keithley 2400 sourcemeter under 1 sun, AM 1.5 G solar simulator (Japan, SAN-EI, XES-40S1). The light intensity of the sun simulation was calibrated by a standard silicon solar cell (certified by NREL) before the testing, giving a value of 100 mW cm<sup>-2</sup> during the test. The current density–voltage ( $J-V$ ) characteristics of hole-only devices were recorded with a Keithley 236 sourcemeter under dark. The external quantum efficiency (EQE) spectra was performed on a commercial EQE measurement system (Beijing, Zolix, DSR 100UV-B).

**Inverted PSCs Fabrication.** The ITO-coated glass substrates were cleaned by sonication in acetone, detergent, deionized water, and isopropyl alcohol and dried in oven at 80 °C for 12 h before used. Then, the ITO substrates were transferred into a N<sub>2</sub> protected glovebox where the H<sub>2</sub>O concentration is  $\leq 0.5$  ppm and O<sub>2</sub> concentration is  $\leq 20$  ppm. The cross-linkable polymer PF<sub>3</sub>N-OX (0.5 mg mL<sup>-1</sup>) was spin-casted from its methanol:acetic acid (99:1 v/v) solution onto the precleaned ITO substrates to form ~5 nm thin film, and the cross-linking process was carried out by heating the half-dried films under 150 °C and fluorescence lamp illumination (no UV lamps required) for 20 min. The solutions for the active layer were prepared by dissolving polymer:PC<sub>71</sub>BM (1:1.5, wt/wt) blend into chlorobenzene:1,8-diiodoctane (97:3 v/v) with polymer concentration at 10 mg/mL. These solutions were heated at 60 °C overnight to completely dissolve the polymer and fullerene. After cooling down to RT and without any filtering, the active layer solutions were spin-coated onto PF<sub>3</sub>N-OX to yield  $110 \pm 10$  nm thick active layers by adjusting the spin-coating speed. After that, about 10 nm molybdenum oxide (MoO<sub>3</sub>) and 100 nm aluminum were thermally deposited on top of the active layer through a shadow mask in a vacuum chamber with base pressure of  $2 \times 10^{-6}$  mbar. The effective area of a device was defined to be 0.16 cm<sup>2</sup> by the shadow mask.

**Hole Mobility Measurement.** Hole-only devices were fabricated with the device structure ITO/PEDOT:PSS(45 nm)/polymer(150 nm)/MoO<sub>3</sub>(10 nm)/Al. The mobility was determined by fitting the dark current to the model of a single carrier SCLC, which is described by the equation

$$J = \frac{9}{8} \epsilon_0 \epsilon_r \mu_h \frac{V^2}{d^3}$$

where  $J$  is the current,  $\mu_h$  is the zero-field mobility,  $\epsilon_0$  is the permittivity of free space,  $\epsilon_r$  is the relative permittivity of the material,  $d$  is the thickness of the active layer, and  $V$  is the effective voltage. The effective voltage can be obtained by subtracting the built-in voltage ( $V_{\text{bi}}$ ) and the voltage drop ( $V_s$ ) from the substrate's series resistance from the applied voltage ( $V_{\text{appl}}$ ),  $V = V_{\text{appl}} - V_{\text{bi}} - V_s$ . The hole-mobility can be calculated from the slope of the  $J^{1/2} \sim V$  curves.

**GIXD Characterization.** Grazing incidence X-ray scattering characterization of the thin films was performed at the Stanford Synchrotron Radiation Lightsource (SSRL) on beam 11-3. The

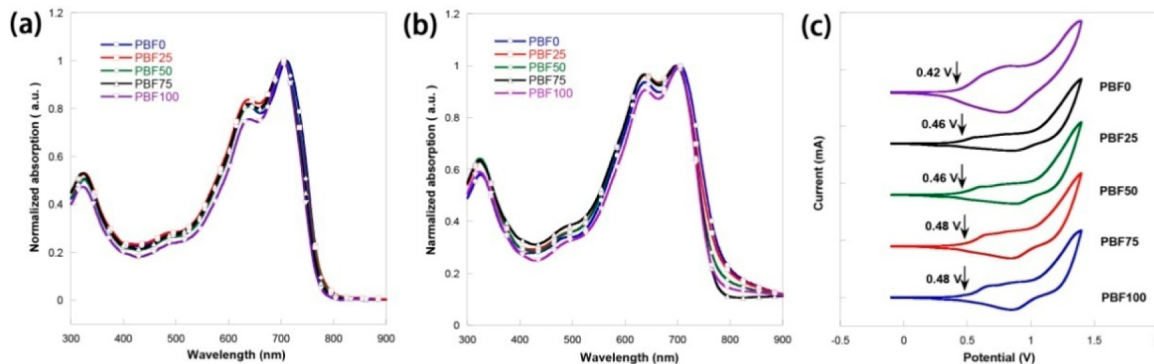


**Figure 2.** UV–vis absorption spectra of PBF<sub>x</sub> polymers in chlorobenzene solution (a) and solid films (b). (c) Cyclic voltammetry curves of the PBF<sub>x</sub> polymers (Potential vs Fc/Fc<sup>+</sup>).

scattering signal was recorded on a 2-D image plate (MAR-345) with a pixel size of 150  $\mu\text{m}$ . The samples were  $\sim$ 15 mm long in the direction of the beam path, and the detector was located at a distance of 450 mm from the sample center (distance calibrated using a lanthanum hexaboride standard). The incidence angle of 0.12° was chosen, which gave the optimized signal-to-background ratio. The beam size was 50 by 150  $\mu\text{m}$ , which resulted in a beam exposure on the sample of 150  $\mu\text{m}$  wide over the entire length of the sample. Typically, a 300 s exposure time was used to collect the diffraction signals. The data was processed and analyzed using WxDiff software package. The (010) peak information is obtained by using Gaussian peaks to fit the diffraction profile (two Gaussians were used with one simulate PCBM peak and another one simulate  $\pi$ – $\pi$  stacking peak).

**RSoXS Characterization.** RSoXS was performed at beamline 11.0.1.2 Lawrence Berkeley National Lab. Thin film samples were spin-casted onto PF<sub>3</sub>N-OX covered SiO<sub>2</sub> wafers. This film preparation process is the same with device fabrication. Then dilute HF solution was used to float the BHJ layer, which was then transferred onto Si<sub>3</sub>N<sub>4</sub> substrate (NorcadiaInc.), and the experiment was done in transition mode. The scattering signals were collected in a vacuum using a Princeton Instrument PI-MTE CCD camera.

**TEM Characterization.** Bright-field transmission electron microscopy studies were conducted with a JEOL 2000 FX TEM operating at an accelerating voltage of 200 kV without any defocus in experiment. The same sample preparation procedure as in RSoXS was used to float the BHJ thin film, which was then collected by copper grid.

## RESULTS AND DISCUSSION

**Synthesis and Characterization.** Figure 1 shows the synthetic procedure used in this study (details in Supporting Information). All the polymers were prepared by Stille polymerization. The two monomers TT and TT-F only differ by the fluorine atom, enabling us to investigate the influence of only the fluorine content on the properties of PBF<sub>x</sub>. Different feed-ratios of TT to TT-F of 100:0, 75:25, 50:50, 25:75, and 0:100 were used. The corresponding copolymers are referred to as PBF0, PBF25, PBF50, PBF75, and PBF100, respectively. All the polymers showed good solubility in common organic solvents and good thermal stability up to 350 °C before degradation (TGA study shown in Supporting Information). The series of PBF<sub>x</sub> polymers had molecular weights varying between 30 and 60 kg/mol, which are considered to be quite

high for low bandgap polymers. Li et al. reported that polymers with molecular weight within this range showed similar performance in the BHJ solar cells, whereas polymers with molecular weight less than 20 kg/mol showed lower performance due to poor packing of the polymers.<sup>51</sup>

**Optical and Electrochemical Properties.** The absorption spectra of the PBF<sub>x</sub> polymers in chlorobenzene (CB) solution and solid films are shown in Figure 2a and b, respectively. In solution all the polymers show a  $\pi$ – $\pi$  transition peak at  $\sim$ 700 nm and a slightly weaker resonance structure peak at  $\sim$ 600 nm. In thin films, the polymers also exhibit similar absorption characteristics with almost no spectral shift of the main peak at 700 nm. The relative intensity of the absorption peak at 600 nm became stronger in thin films, indicating an H-type aggregation of the main chain.<sup>52</sup> The relative intensities of the 600 and 700 nm peaks varied slightly between the different polymers, suggesting that the packing of the polymers was affected by the fluorine content. The onset of the thin film absorption blue-shifted slightly as the fluorine content increased, indicating a small increase in the optical band gaps (Table 1). Cyclic

**Table 1. Physical Properties of PBF<sub>x</sub> Polymers**

polymer	M <sub>n</sub> /PDI [kDa] <sup>a</sup>	Film E <sub>g</sub> [eV] <sup>b,g</sup>	absolute coefficient [cm <sup>-1</sup> ] <sup>c</sup>	IP [eV] <sup>d</sup>	EA [eV] <sup>e</sup>
PBF0	34/2.2	1.57	6.2 × 10 <sup>4</sup>	5.22	3.65
PBF25	51/2.4	1.59	6.6 × 10 <sup>4</sup>	5.26	3.67
PBF50	52/2.5	1.60	6.4 × 10 <sup>4</sup>	5.26	3.66
PBF75	40/2.9	1.60	6.0 × 10 <sup>4</sup>	5.28	3.68
PBF100	32/2.7	1.61	5.6 × 10 <sup>4</sup>	5.28	3.67

<sup>a</sup>Determined by GPC (1,2,4-trichlorobenzene) against PS standards.

<sup>b</sup>Band gap calculated from the onset of the absorption of the solid film. <sup>c</sup>Measured from film absorption spectra at  $\lambda_{\text{max}}$ . <sup>d</sup>Measured by cyclicvoltammetry. <sup>e</sup>Determined from IP – E<sub>g</sub>.

voltammetry was used to study the energy levels of the polymers (Figure 2c). The IP values were estimated from the onset of the oxidation peak vs SCE in the voltammogram and calculated by the equation of IP = e[E<sub>ox</sub> – E<sub>ox</sub>(Fc/Fc<sup>+</sup>) + 4.80]. The fluorine substitution slightly increases the IP of the polymers, with a difference of 0.06 eV obtained between the highest fluorinated and the nonfluorinated polymers. The approximate EA values of these copolymers were estimated from the difference between the IP values and E<sub>g</sub><sup>opt</sup> and are almost identical at 3.66 eV.<sup>50</sup>

**Photovoltaic Properties.** Bulk heterojunction (BHJ) solar cells using these polymers as the electron donors and PC<sub>71</sub>BM

as the electron acceptor were fabricated in an inverted geometry by using our newly developed poly[9,9-bis(3'-(*N,N*-dimethylamino)propyl)-2,7-fluorene]-*alt*-2,7-(9,9-bis(3-ethyl(oxetane-3-ethoxy)hexyl)fluorene)] ( $\text{PF}_3\text{N-OX}$ ) as the cathode buffer layer. The cross-linked  $\text{PF}_3\text{N-OX}$  interfacial layer could effectively modify the electronic properties of ITO and improve electron extraction property, with the additional benefit of enhanced device stability.<sup>53–58</sup>  $\text{MoO}_3/\text{Al}$  was used as the anode for the inverted cells. The active layer blends (polymer:PC<sub>71</sub>BM = 1:1.5 w/w after optimization) were processed from either pure chlorobenzene solution or chlorobenzene solution with 3 vol % of 1,8-diiodooctane (DIO) as processing additive to optimize the morphology.

The current density–voltage ( $J$ – $V$ ) curves and the performance of the devices processed from CB:DIO are shown in Figure 3a and Table 2, respectively. The  $J$ – $V$  curves and the

device data processed from pure chlorobenzene are summarized in the Supporting Information. The  $V_{\text{oc}}$  of the BHJ solar cells increased with fluorine content in the polymers due to the deepening of the HOMO levels,<sup>59,60</sup> which is in agreement with our materials design principle. PBF100 showed a  $V_{\text{oc}}$  of 0.79 eV, which is 0.07 eV larger than that obtained from the nonfluorinated PBF0. This value is among the highest for this class of polymers. The  $J_{\text{sc}}$  of all the BHJ devices are close to 17  $\text{mA}/\text{cm}^2$ , which indicates that the light harvesting properties of the polymers are quite similar. The hole mobility of the copolymers was examined by the space charge limited current (SCLC) method in single carrier devices. As shown in Table 2, increasing fluorine content enhances the hole mobility of the BHJ films from  $9.27 \times 10^{-6} \text{ cm}^2 \text{ V}^{-1} \text{ s}^{-1}$  (PBF0) to  $2.75 \times 10^{-5} \text{ cm}^2 \text{ V}^{-1} \text{ s}^{-1}$  (PBF100). Figure 3b shows the external quantum efficiency (EQE) curves of the polymer:PC<sub>71</sub>BM blends; the  $J_{\text{sc}}$  calculated from the integrated value of the EQE spectrum was in good agreement with the device results. All the PBF<sub>x</sub> polymers exhibited a broad response range, whereas PBF0 showed more effective solar energy harvesting capabilities in the short-wavelength range. PBF100 showed a slightly higher EQE compared to other fluorinated materials, thus yielding a slightly larger  $J_{\text{sc}}$  value. The PBF0-based devices showed a moderate FF of 56.7% due to the relatively low hole mobility in the BHJ. For the fluorine-containing polymers, an obvious trend of increasing FF with the fluorine content was observed from 54.2% for PBF25 to 65.2% for PBF100. The increase in the FF can be attributed to the gradual increase in hole mobility of the BHJ films with increasing fluorine content of the polymers. Another factor that will affect the FF is the film morphology, nanostructured film with optimized morphology is desirable to promote exciton dissociation and reduce charge recombination, leading to higher FF. By controlling the morphology with the fluorine content of the polymers, a significant improvement of both the  $V_{\text{oc}}$  and FF was achieved, increasing the PCE from 6.99% for PBF0-based devices to 8.75% for the PBF100-based devices.

**GIXD Characterization.** To study the effect of fluorination of the polymers on the morphology of the BHJ blends, a combination of the structural characterization techniques were employed. First, grazing incidence X-ray diffraction (GIXD) was used to study the structural order of these polymers in pristine thin films and blended films (processed from CB and CB:DIO mixture). The experiments were performed at the Stanford Synchrotron Radiation Laboratory (SSRL) on beamline 11-3 using a 2-D image plate (MAR-345) at an incidence angle of  $0.12^\circ$ . The data was processed and analyzed using WxDiff software package.<sup>61</sup> As seen from Figure 4a and Supporting Information Figure S5, a face-on orientation was found for all the pure PBF<sub>x</sub> thin films, with evident (010)  $\pi-\pi$  stacking reflection in the out-of-plane direction and the (100)

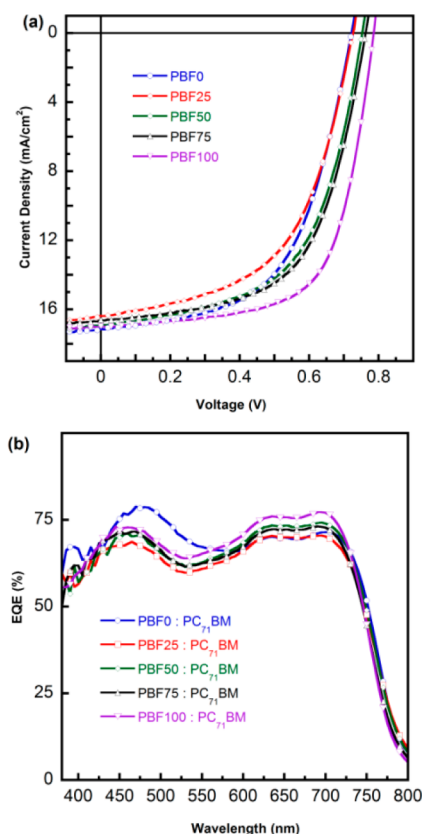


**Figure 3.** (a) Current–voltage characteristics of polymer solar cells for each polymer under simulated AM1.5G illumination ( $100 \text{ mW cm}^{-2}$ ). (b) External quantum efficiency curves of the devices for each polymer.

**Table 2. Photovoltaic Performances of Devices with  $\text{PBF}_x:\text{PC}_{71}\text{BM}$  (Weight Ratio of 1:1.5) under the Illumination of AM 1.5 G,  $100 \text{ mW cm}^{-2}$ <sup>a</sup>**

polymer	$J_{\text{sc}}$ ( $\text{mA}/\text{cm}^2$ )	$V_{\text{oc}}$ (V)	FF (%)	PCE (%) (max)	mobility ( $\text{cm}^2 \text{ V}^{-1} \text{ s}^{-1}$ )
PBF0	$16.69 \pm 0.37$	$0.72 \pm 0.01$	$56 \pm 2$	$6.69 \pm 0.30(6.99)$	$9.27 \times 10^{-6}$
PBF25	$16.19 \pm 0.23$	$0.73 \pm 0.01$	$54 \pm 1$	$6.38 \pm 0.10(6.48)$	$1.29 \times 10^{-5}$
PBF50	$16.63 \pm 0.28$	$0.75 \pm 0.01$	$57 \pm 1$	$7.01 \pm 0.30(7.31)$	$1.36 \times 10^{-5}$
PBF75	$16.32 \pm 0.31$	$0.76 \pm 0.01$	$59 \pm 3$	$7.28 \pm 0.25(7.53)$	$1.48 \times 10^{-5}$
PBF100	$16.74 \pm 0.14$	$0.79 \pm 0.01$	$63 \pm 2$	$8.36 \pm 0.39(8.75)$	$2.75 \times 10^{-5}$

<sup>a</sup>Above were average values and the corresponding standard deviations were calculated over eight devices.

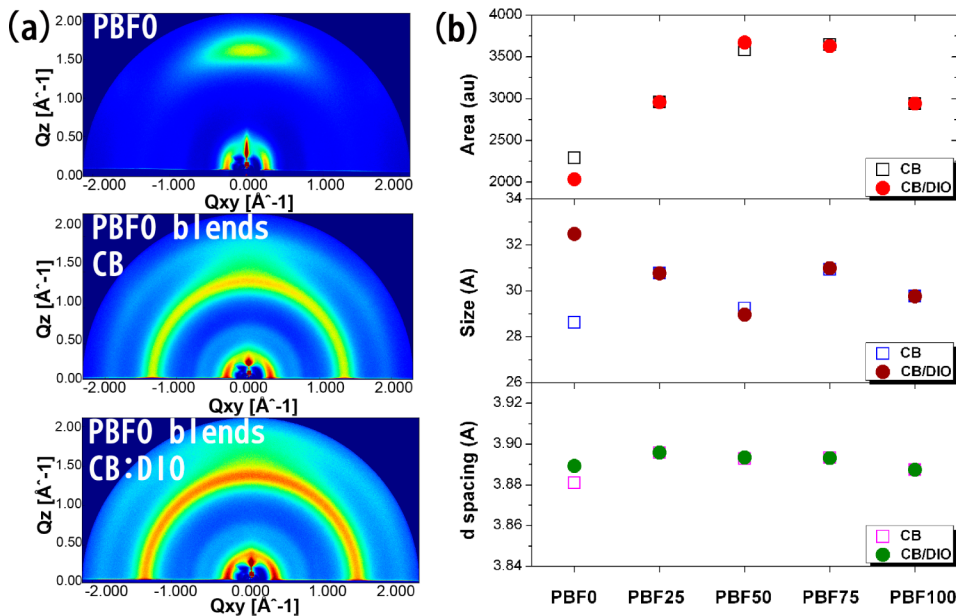


**Figure 4.** (a) Typical GIXD scattering images of  $\text{PBF}_x$  polymers and blends. (b) Analyzed data from (010) peak of GIXD results of blend films.

lamellar  $d$ -spacing reflection in the in-plane direction. With the polymer:PCBM blends, the diffraction arising from the PCBM overlaps the (010) reflection; consequently, peak fitting routines had to be used to extract detailed structural information, the broad peak distribution and the weak or even absence of the higher reflections indicate that the polymers are not highly ordered. For all the polymers and their blends, the (100) reflection fixed at  $q \sim 0.25 \text{ \AA}^{-1}$  corresponding to a  $d$ -spacing of 2.5 nm, which indicated addition of fluorine does not alter  $d$ -spacing significantly. This  $d$ -spacing is determined by the alkyl-thienyl group on the BDT unit, and correlates well with previous publications.<sup>40</sup> Detailed analyses of the (010)  $\pi-\pi$  stacking peak in the blends are summarized in Figure 4b (line-cut profiles in the out-of-plane direction are shown in Supporting Information Figure S6.) to show the influence of fluorine modification on structural changes in the films. As can be seen, a  $\pi-\pi$  stacking distance of  $\sim 3.89 \text{ \AA}$  and a (010) "crystal size" between 28 to 33  $\text{\AA}$  (determined from the Scherrer equation) are seen for all the blends, both showing almost no changes with fluorine content variation. Compared to the crystal size of  $\sim 20 \text{ \AA}$  found in the commonly studied PTB7:PCBM blend,<sup>62</sup> the (010) crystal size of  $\sim 30 \text{ \AA}$  for our polymers is slightly larger, corresponding to a stack of 7–8 layers. The increased crystal size of the polymers can be attributed to the enhanced  $\pi-\pi$  interaction induced by the alkylthienyl side chain.<sup>40</sup> The integrated area under the (010) peak was used to determine a relative crystallinity of the  $\text{PBF}_x$  polymers in the blends. The relative crystallinity was found to increase with increasing fluorine content up to PBF50 and then decrease with further increase in the fluorine content. This is probably due to the enhanced  $\pi$ -stacking interactions between the polymers, as quadrupolar interactions can be formed between adjacent fluorine-substituted thiophene moieties, which contains an electron-deficient fluorinated aromatic ring and an electron-rich nonfluorinated ring,<sup>38</sup> and the exception for PBF100 may arise from the relatively lower molecular weight.<sup>51,63</sup> The thin films processed from CB and CB:DIO yielded similar results, indicating that the solvent additive did not affect the crystalline structure of these

materials. Although the PBF50 and PBF75 show the highest relative crystallinity with more  $\pi-\pi$  stacking in the out-of-plane direction of the blend film, the corresponding hole mobilities are lower than that of the PBF100. This indicates that crystallinity cannot be the sole factor influencing the charge transport properties and performance of the devices. Other factors, like connectivity between the crystallites, may also be important because the charges must be transported across the entire thickness of the film before they can be collected by the electrodes. The higher hole mobilities in the case of PBF100 blends, despite the lower crystallinity, may be attributed to the formation of continuous charge transport pathways in the BHJ film. On the whole, the fluorine substitution does not significantly change the lamellar  $d$ -spacing,  $\pi-\pi$  stacking distance and (010) crystal size of the polymers but increases the relative crystallinity of the polymers in the blends; together with a better connectivity between the crystallites, all these make fully fluorinated PBF100 show the highest hole mobility.

**TEM Characterization.** Transmission electron microscopy (TEM) was used to provide real-space images of the morphologies of the  $\text{PBF}_x$ :PCBM blends cast from CB and CB:DIO. Thin films processed from chlorobenzene contained large aggregates of PCBM (Figure 5). In the PBF0:PCBM blends, some PCBM aggregates were even  $\sim 300 \text{ nm}$  in size. The average center-to-center spacing between the aggregates was  $\sim 300 \text{ nm}$ . In the case of fluorinated polymer blends, the PCBM aggregates became slightly smaller but had a higher areal density. When the blend films were cast from CB:DIO, the films became smoother with phase separation on the tens of nanometers size scale. Consequently, the additive is regulating the size of the morphology by solubilizing the PCBM, allowing the polymer to come out of solution initially and then allowing the PCBM to come out of solution in a matrix defined by the polymer, in agreement with other reports.<sup>64–66</sup>

**RSoXS Characterization.** Scattering methods provide a statistical view of the phase separation that complements results from TEM.<sup>67</sup> Resonant soft X-ray scattering (RSoXS) utilizing the unique optical contrast between polymer and fullerene at the carbon edge (284.2 eV) for the thin films are summarized

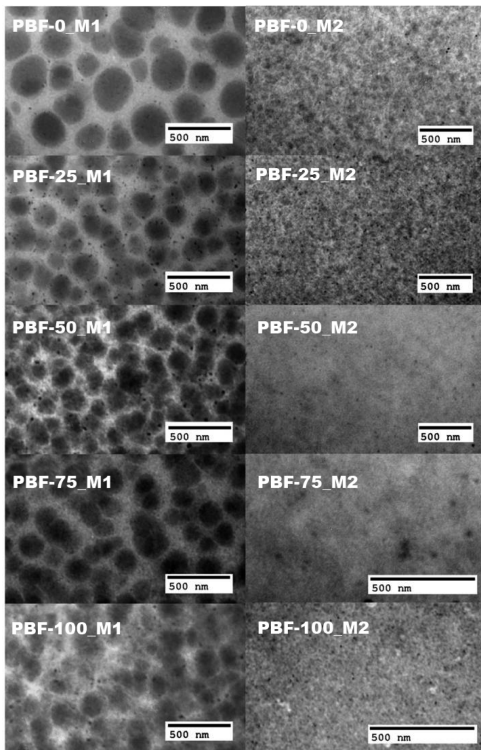


**Figure 5.** TEM images of  $\text{PBF}_x\text{:PCBM}$  blends processed from chlorobenzene and chlorobenzene:DIO mixture. (M1 denotes chlorobenzene processed thin films; M2 denotes chlorobenzene:DIO processed thin films.)

in Figure 6. For the CB-cast films, the interferences observed clearly indicate a characteristic length scale of several hundred nanometers ( $2\pi/q$ ). PBF0 blends showed a length scale of 285 nm, which correlates well with TEM characterization. PBF100 blends showed a feature size of 185 nm. In between these two polymers, the size of the phase separated domains decreased in proportion to the fluorine content of the polymer (Figure 6a). When the films were cast from CB:DIO, the characteristic length scale was reduced to tens of nanometers and also kept a

decreasing trend with the increasing fluorine content of the polymers (Figure 6b). In these blends, the morphology consists of PCBM aggregates imbedded in a polymer rich matrix and can be treated as a two-phase system, so the scattering actually originates from optical contrast between polymer-rich and fullerene-rich domains. In view of this,  $I(q)q^2$  as a integrating function of  $q$  in Figure 6a and b, a measure of the scattering power of the system, is shown in Figures 6c. For both the CB and CB:DIO cases, a reduction in the total scattering power along with the increasing fluorine content was seen. However, the origins of this reduction are different in the two cases. For the CB cast films, a large size scale structure is seen, consistent with the electron microscopy results, due to the formation of PCBM domains. The relative solubilities of the fluorinated polymers and PCBM in CB can describe the reduction in the scattering power. With increasing concentration of fluorine in the polymer, the solubility decreases and, as such, will come out of solution earlier during the solvent evaporation and compete with the PCBM, which leads to the size scale of these domain decreasing. The integrated scattering is independent of the size and shape of the domains, and the continuous decrease with increasing fluorine concentration indicates that the contrast between polymer-rich and fullerene-rich domains in the system, arising from the average electron densities of the domains, is decreasing. This is consistent with the relative rates at which the PCBM and polymer come out of solution. As for CB:DIO cast films, the total scattering decreases along with the characteristic length scale of the morphology, but the average crystal size, as reflected by the width of the (010) reflection, remains relatively constant. This indicates that the polymer crystallizes from solution, forming a network structure, with a mesh-size reflected in the interference maximum, where crystallinity, that is, the total amount of the fluorinated polymer in the crystalline phase, increases. The remaining PCBM and polymer fill in the space between the fibrillar network causing the electron density of the mixture to increase, giving rise to a reduction in the total integrated scattering. As the concentration of fluorine in the polymer exceeds  $\sim 50\%$ , this crystal size remains relatively constant, the effective network size continues to decrease, from  $\sim 90$  nm for PBF0 to  $\sim 60$  nm for

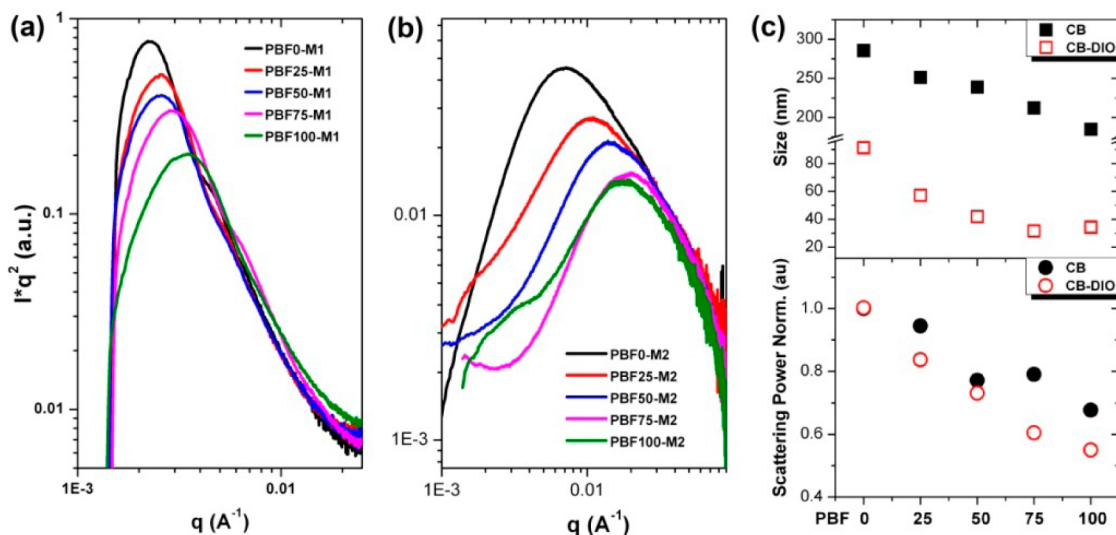


**Figure 6.** (a) RSoXS profiles of chlorobenzene processed thin film blends. (b) RSoXS profiles of chlorobenzene:DIO processed thin film blends. (c) Feature size of phase separation and scattering power of blended thin films.

PBF25 to  $\sim$ 40 nm for PBF50 to  $\sim$ 30 nm for PBF75 and PBF100, which indicates more sufficient interpenetration of polymer and PCBM in the film with increasing fluorine content. As with the blends cast from only CB, the reduction in the characteristic length scale of the morphology leads to an increase in the interfacial area, which usually leads to a larger  $J_{sc}$ . This was not the case here, though, since the difference in  $J_{sc}$  between the devices was quite small. Consequently, as with the mixtures cast from only CB, the size scale of the morphology is only one parameter that is varying and one must, also, consider the total crystallinity in the system and the distribution of the components within the domains. With increasing fluorine content of the polymer, the gradually improved solar cell performance can, therefore, be attributed to the enhanced  $V_{oc}$  and more balanced charge transport due to the reduced size scale and more effective crystalline network for component distribution within the domains, which yielded a better FF.

## CONCLUSIONS

In conclusion, we have synthesized a series of benzodithiophene-thienothiophene copolymers with different amounts of fluorine decoration. We observed that incorporating fluorine into the thienothiophene units could deepen the HOMO energy levels without significantly influencing the bandgap and the light harvesting properties of the polymers. As a result, an improved  $V_{oc}$  in OPV devices was achieved while the high  $J_{sc}$  was retained. The FFs of the devices were found to be strongly depending on the morphology and charge transport properties in the BHJ films. Improved morphology with phase separation length scale in the tens of nanometers can be achieved by casting the films with solvent additive. It was also found that the size of phase separation further decreases with increasing fluorine content possibly due to the interactions of the polymer and PCBM with the casting solvent and additive. Although the reduction in the size scale of the phase separated morphology with increasing fluorine content in the polymers is in good agreement with the improved PCE of the corresponding devices, the in-depth structural and electrical analysis performed in our study indicate that other factors, such as the polymer crystallinity, distribution of components within the domains, and charge transport property, also affect the ultimate device efficiency. These findings provide new insights to evaluate the structure–property–performance relationship in polymer solar cells and lead toward better design criteria for photovoltaic materials.

## ASSOCIATED CONTENT

### Supporting Information

TGA plots of copolymers, DSC scan curves, the  $J^{1/2}$  vs  $V$  plots of mobility measurement of polymers, GIXD images, line-cut profiles, and so forth. This material is available free of charge via the Internet at <http://pubs.acs.org>.

## AUTHOR INFORMATION

### Corresponding Authors

\*E-mail: msangusyip@scut.edu.cn. (H.-L. Y.)

\*E-mail: msfhuang@scut.edu.cn. (F. H.)

\*E-mail: russell@mail.pse.umass.edu. (T. P. R.)

### Author Contributions

<sup>†</sup>These authors contributed equally.

### Notes

The authors declare no competing financial interest.

## ACKNOWLEDGMENTS

This work was financially supported by the Ministry of Science and Technology (No. 2014CB643501), the Natural Science Foundation of China (No. 21125419, 50990065 and S1010003), and the Guangdong Natural Science Foundation (No. S2012030006232). Structural characterization of the materials was supported by the Department of Energy-supported Energy Frontier Research Center at the University of Massachusetts (DE-SC0001087). GIWAXS was performed at the Stanford Synchrotron Radiation Light Source (SSRL) on beam 11-3, R-SoXS was performed at beamline 11.0.1.2 at the Advanced Light Source, Berkeley National Laboratory, which are supported by the DOE, Office of Science, and Office of Basic Energy Sciences.

## REFERENCES

- (1) Sariciftci, N. S.; Smilowitz, L.; Heeger, A. J.; Wudl, F. *Science* **1992**, 258, 1474.
- (2) Darling, S. B.; You, F. Q. *RSC Adv.* **2013**, 3, 17633.
- (3) Dennler, G.; Scharber, M. C.; Brabec, C. J. *Adv. Mater.* **2009**, 21, 1323.
- (4) Chochos, C. L.; Choulis, S. A. *Prog. Polym. Sci.* **2011**, 36, 1326.
- (5) Brabec, C. J.; Gowrisanker, S.; Halls, J. J. M.; Laird, D.; Jia, S. J.; Williams, S. P. *Adv. Mater.* **2010**, 22, 3839.
- (6) Havinga, E. E.; Hoeve, W. T.; Wynberg, H. *Synth. Met.* **1993**, 55, 299.
- (7) Li, G.; Zhu, R.; Yang, Y. *Nat. Photonics* **2012**, 6, 153.
- (8) Chen, J. W.; Cao, Y. *Acc. Chem. Res.* **2009**, 42, 1709.
- (9) Uy, R. L.; Price, S. C.; You, W. *Macromol. Rapid Commun.* **2012**, 33, 1162.
- (10) Hou, J. H.; Park, M. H.; Zhang, S. Q.; Yao, Y.; Chen, L. M.; Li, J. H.; Yang, Y. *Macromolecules* **2008**, 41, 6012.
- (11) Chen, H. Y.; Hou, J. H.; Zhang, S. Q.; Liang, Y. Y.; Yang, G. W.; Yang, Y.; Yu, L. P.; Wu, Y.; Li, G. *Nat. Photonics* **2009**, 3, 649.
- (12) Hou, J. H.; Tan, Z. A.; Yan, Y.; He, Y. J.; Yang, C. H.; Li, Y. F. *J. Am. Chem. Soc.* **2006**, 128, 4911.
- (13) Huang, F.; Chen, K. S.; Yip, H. L.; Hau, S. K.; Acton, O.; Zhang, Y.; Luo, J. D.; Jen, A. K. Y. *J. Am. Chem. Soc.* **2009**, 131, 13886.
- (14) Son, H. J.; Wang, W.; Xu, T.; Liang, Y. Y.; Wu, Y.; Li, G.; Yu, L. P. *J. Am. Chem. Soc.* **2011**, 133, 1885.
- (15) Schroeder, B. C.; Ashraf, R. S.; Thomas, S.; White, A. J. P.; Biniek, L.; Nielsen, C. B.; Zhang, W. M.; Huang, Z. G.; Tuladhar, P. S.; Watkins, S. E.; Anthopoulos, T. D.; Durrant, J. R.; McCulloch, I. *Chem. Commun.* **2012**, 48, 7699.
- (16) Fei, Z. P.; Shahid, M.; Yaacobi-Gross, N.; Rossbauer, S.; Zhong, H. L.; Watkins, S. E.; Anthopoulos, T. D.; Heeney, M. *Chem. Commun.* **2012**, 48, 11130.
- (17) Albrecht, S.; Janietz, S.; Schindler, W.; Frisch, J.; Kurpiers, J.; Kniepert, J.; Inal, S.; Pingel, P.; Fostirooulos, K.; Koch, N.; Neher, D. *J. Am. Chem. Soc.* **2012**, 134, 14932.
- (18) Price, S. C.; Stuart, A. C.; Yang, L. Q.; Zhou, H. X.; You, W. *J. Am. Chem. Soc.* **2011**, 133, 4625.
- (19) Liang, Y. Y.; Xu, Z.; Xia, J. B.; Tsai, S. T.; Wu, Y.; Li, G.; Ray, C.; Yu, L. P. *Adv. Mater.* **2010**, 22, E135.
- (20) Zhou, H. X.; Yang, L. Q.; Stuart, A. C.; Price, S. C.; Liu, S. B.; You, W. *Angew. Chem., Int. Ed.* **2011**, 50, 2995.
- (21) Li, Z.; Lu, J. P.; Tse, S. C.; Zhou, J. Y.; Du, X. M.; Tao, Y.; Ding, J. F. *J. Mater. Chem.* **2011**, 21, 3226.
- (22) Zhang, Y.; Chien, S. C.; Chen, K. S.; Yip, H. L.; Sun, Y.; Davies, J. A.; Chen, F. C.; Jen, A. K. Y. *Chem. Commun.* **2011**, 47, 11026.
- (23) Zhang, Y.; Zou, J. Y.; Cheuh, C. C.; Yip, H. L.; Jen, A. K. Y. *Macromolecules* **2012**, 45, 5427.
- (24) Peng, Q.; Liu, X. J.; Su, D.; Fu, G. W.; Xu, J.; Dai, L. M. *Adv. Mater.* **2011**, 23, 4554.
- (25) Schroeder, B. C.; Huang, Z. G.; Ashraf, R. S.; Smith, J.; D'Angelo, P.; Watkins, S. E.; Anthopoulos, T. D.; Durrant, J. R.; McCulloch, I. *Adv. Funct. Mater.* **2012**, 22, 1663.

- (26) Zhou, H. X.; Yang, L. Q.; You, W. *Macromolecules* **2012**, *45*, 607.
- (27) Bronstein, H.; Frost, J. M.; Hadipour, A.; Kim, Y. J.; Nielsen, C. B.; Ashraf, R. S.; Rand, B. P.; Watkins, S.; McCulloch, I. *Chem. Mater.* **2013**, *25*, 277.
- (28) Stuart, A. C.; Tumbleston, J. R.; Zhou, H. X.; Li, W. T.; Liu, S. B.; Ade, H.; You, W. *J. Am. Chem. Soc.* **2013**, *135*, 1806.
- (29) Yu, G.; Gao, J.; Hummelen, J. C.; Wudl, F.; Heeger, A. J. *Science* **1995**, *270*, 1789.
- (30) Carsten, B.; Szarko, J. M.; Son, H. J.; Wang, W.; Lu, L. Y.; He, F.; Rolczynski, B. S.; Lou, S. J.; Chen, L. X.; Yu, L. P. *J. Am. Chem. Soc.* **2011**, *133*, 20468.
- (31) Rolczynski, B. S.; Szarko, J. M.; Son, H. J.; Liang, Y. Y.; Yu, L. P.; Chen, L. X. *J. Am. Chem. Soc.* **2012**, *134*, 4142.
- (32) Zang, H. D.; Liang, Y. Y.; Yu, L. P.; Hu, B. *Adv. Energy Mater.* **2011**, *1*, 923.
- (33) Dou, L. T.; Chen, C. C.; Yoshimura, K.; Ohya, K.; Chang, W. H.; Gao, J.; Liu, Y. S.; Richard, E.; Yang, Y. *Macromolecules* **2013**, *46*, 3384.
- (34) Chen, H. C.; Chen, Y. H.; Liu, C. C.; Chien, Y. C.; Chou, S. W.; Chou, P. T. *Chem. Mater.* **2012**, *24*, 4766.
- (35) Liao, S. H.; Jhuo, H. J.; Cheng, Y. S.; Chen, S. A. *Adv. Mater.* **2013**, *25*, 4766.
- (36) He, Z. C.; Zhong, C. M.; Su, S. J.; Xu, M.; Wu, H. B.; Cao, Y. *Nat. Photonics* **2012**, *6*, 591.
- (37) Chen, W.; Nikiforov, M. P.; Darling, S. B. *Energy Environ. Sci.* **2012**, *5*, 8045.
- (38) Liang, Y. Y.; Feng, D. Q.; Wu, Y.; Tsai, S. T.; Li, G.; Ray, C.; Yu, L. P. *J. Am. Chem. Soc.* **2009**, *131*, 7792.
- (39) Chen, W.; Xu, T.; He, F.; Wang, W.; Wang, C.; Strzalka, J.; Liu, Y.; Wen, J. G.; Miller, D. J.; Chen, J. H.; Hong, K. L.; Yu, L. P.; Darling, S. B. *Nano Lett.* **2011**, *11*, 3707.
- (40) Huang, Y.; Guo, X.; Liu, F.; Huo, L. J.; Chen, Y. N.; Russell, T. P.; Han, C. C.; Li, Y. F.; Hou, J. H. *Adv. Mater.* **2012**, *24*, 3383.
- (41) Li, X. H.; Choy, W. C. H.; Huo, L. J.; Xie, F. X.; Sha, W. E. I.; Ding, B. F.; Guo, X.; Li, Y. F.; Hou, J. H.; You, J. B.; Yang, Y. *Adv. Mater.* **2012**, *24*, 3046.
- (42) Huo, L. J.; Zhang, S. Q.; Guo, X.; Xu, F.; Li, Y. F.; Hou, J. H. *Angew. Chem., Int. Ed.* **2011**, *50*, 9697.
- (43) Dou, L. T.; Gao, J.; Richard, E.; You, J. B.; Chen, C. C.; Cha, K. C.; He, Y. J.; Li, G.; Yang, Y. *J. Am. Chem. Soc.* **2012**, *134*, 10071.
- (44) Lim, D. C.; Kim, K. D.; Park, S. Y.; Hong, E. M.; Seo, H. O.; Lim, J. H.; Lee, K. H.; Jeong, Y.; Song, C.; Lee, E.; Kim, Y. D.; Cho, S. *Energy Environ. Sci.* **2012**, *5*, 9803.
- (45) Park, H. Y.; Lim, D. G.; Kim, K. D.; Jang, S. Y. *J. Mater. Chem. A* **2013**, *1*, 6327.
- (46) Wang, H. X.; Yu, X. F.; Yi, C.; Ren, H.; Liu, C.; Yang, Y. L.; Xiao, S.; Zheng, J.; Karim, A.; Cheng, S. Z. D.; Gong, X. *J. Phys. Chem. C* **2013**, *117*, 4358.
- (47) He, F.; Wang, W.; Chen, W.; Xu, T.; Darling, S. B.; Strzalka, J.; Liu, Y.; Yu, L. P. *J. Am. Chem. Soc.* **2011**, *133*, 3284.
- (48) Huo, L. J.; Hou, J. H.; Chen, H. Y.; Zhang, S. Q.; Jiang, Y.; Chen, T. L.; Yang, Y. *Macromolecules* **2009**, *42*, 6564.
- (49) Li, Y. F.; Cao, Y.; Gao, J.; Wang, D. L.; Yu, G.; Heeger, A. J. *Synth. Met.* **1999**, *99*, 243.
- (50) Bredas, J.- L. *Mater. Horiz.* **2014**, *1*, 17.
- (51) Li, W. T.; Yang, L. Q.; Tumbleston, J. R.; Yan, L.; Ade, H.; You, W. *Adv. Mater.* **2014**, DOI: 10.1002/adma.201305251.
- (52) Liu, F.; Gu, Y.; Wang, C.; Zhao, W.; Chen, D.; Briseno, A. L.; Russell, T. P. *Adv. Mater.* **2012**, *24*, 3947.
- (53) Zhang, K.; Guan, X.; Huang, F.; Cao, Y. *Acta Chim. Sin.* **2012**, *70*, 2489.
- (54) Liu, S. J.; Zhang, Z. P.; Chen, D. C.; Duan, C. H.; Lu, J. M.; Zhang, J.; Huang, F.; Su, S. J.; Chen, J. W.; Cao, Y. *Sci. China: Chem.* **2013**, *43*, 437.
- (55) Hsieh, C. H.; Cheng, Y. J.; Li, P. J.; Chen, C. H.; Dubosc, M.; Liang, R. M.; Hsu, C. S. *J. Am. Chem. Soc.* **2010**, *132*, 4887.
- (56) Liu, S. J.; Zhong, C. M.; Zhang, J.; Duan, C. H.; Hu, X. W.; Huang, F. *Sci. China: Chem.* **2011**, *54*, 1745.
- (57) Zhong, C. M.; Liu, S. J.; Huang, F.; Wu, H. B.; Cao, Y. *Chem. Mater.* **2011**, *23*, 4870.
- (58) Dong, Y.; Hu, X. W.; Duan, C. H.; Liu, P.; Liu, S. J.; Lan, L. Y.; Chen, D. C.; Ying, L.; Su, S. J.; Gong, X.; Huang, F.; Cao, Y. *Adv. Mater.* **2013**, *25*, 3683.
- (59) Brabec, C. J.; Cravino, A.; Meissner, D.; Sariciftci, N. S.; Fromherz, T.; Rispens, M. T.; Sanchez, L.; Hummelen, J. C. *Adv. Funct. Mater.* **2001**, *11*, 374.
- (60) Gadisa, A.; Svensson, M.; Andersson, M. R.; Inganäs, O. *Appl. Phys. Lett.* **2004**, *84*, 1609.
- (61) Mannsfeld, S. C. B.; Virkar, A.; Reese, C.; Toney, M. F.; Bao, Z. *Adv. Mater.* **2009**, *21*, 2294.
- (62) Collins, B. A.; Li, Z.; Tumbleston, J. R.; Gann, E.; McNeill, C. R.; Ade, H. *Adv. Energy Mater.* **2013**, *3*, 65.
- (63) Chu, T. Y.; Lu, J. P.; Beaupre, S.; Zhang, Y. G.; Pouliot, J. R.; Zhou, J. Y.; Najari, A.; Leclerc, M.; Tao, Y. *Adv. Funct. Mater.* **2012**, *22*, 2345.
- (64) Liao, H. C.; Ho, C. C.; Chang, C. Y.; Jao, M. H.; Darling, S. B.; Su, W. F. *Mater. Today* **2013**, *16*, 326.
- (65) Lee, J. K.; Ma, W. L.; Brabec, C. J.; Yuen, J.; Moon, J. S.; Kim, J. Y.; Lee, K.; Bazan, G. C.; Heeger, A. J. *J. Am. Chem. Soc.* **2008**, *130*, 3619.
- (66) Lou, S. J.; Szarko, J. M.; Xu, T.; Yu, L. P.; Marks, T. J.; Chen, L. X. *J. Am. Chem. Soc.* **2011**, *133*, 20661.
- (67) Gann, E.; Young, A. T.; Collins, B. A.; Yan, H.; Nasiatka, J.; Padmore, H. A.; Ade, H.; Hexemer, A.; Wang, C. *Rev. Sci. Instrum.* **2012**, *83*, 045110.